Accepted Article

Title: Conversion of γγ-Valerolactone to ethyl valerate over metal promoted Ni/ZSM-5 catalysts: Influence of Ni0/Ni2+ heterojunctions on activity and product selectivity

Authors: Vijay Kumar Velisoju, Deshetti Jampaiah, Naresh Gutta, Ursula Bentrup, Angelika Brückner, Sureh K. Bhargava, and Venugopal Akula

This manuscript has been accepted after peer review and appears as an Accepted Article online prior to editing, proofing, and formal publication of the final Version of Record (VoR). This work is currently citable by using the Digital Object Identifier (DOI) given below. The VoR will be published online in Early View as soon as possible and may be different to this Accepted Article as a result of editing. Readers should obtain the VoR from the journal website shown below when it is published to ensure accuracy of information. The authors are responsible for the content of this Accepted Article.

FULL PAPER

Conversion of γ-Valerolactone to ethyl valerate over metal promoted Ni/ZSM-5 catalysts: Influence of Ni⁰/Ni²⁺ heterojunctions on activity and product selectivity

Vijay Kumar Velisoju,*[a] Deshetti Jampaiah,[b] Naresh Gutta,[c] Ursula Bentrup,*[a] Angelika Brückner,[a] Suresh K. Bhargava,[b] Venugopal Akula*[c]

Abstract: Promoter (Cr, Mo and W) modified Ni/ZSM-5 catalysts were explored in the vapor phase conversion of γ-valerolactone (GVL) to ethyl valerate (EV; gasoline blender) at atmospheric pressure. Among the three different promoters (Cr, Mo and W) tested the Mo-modified catalyst was found to be the best candidate. In addition, this catalyst was found to be stable up to 50 h reaction time with an insignificant decrease in activity. The good catalytic performance is related to an optimal ratio of acid and hydrogenation functions provided by Ni²⁺ and Ni⁰, respectively. *In situ* FTIR spectroscopic studies revealed a strong adsorption of GVL on all catalysts which quickly reacts with dosed ethanol by formation of EV, most pronounced on the Mo-modified catalyst, while VA was identified as side product. These findings suggest the preferred GVL ring opening by cracking the C–O bond on the methyl side of the GVL molecule on this type of catalysts leading to pentenioic acid as intermediate, which is quickly hydrogenated and esterified.

Introduction

Catalysts containing two active metal components have been widely studied in different reactions *e.g.* CO₂ methanation, catalytic hydrotreating of bio-liquids and CO oxidation, owing to their improved activity and selectivity toward the desired products.[1-3] Recent analyses revealed unprecedented activity of dual metal components in the reduction reactions as compared to their monometallic counterparts.[4-6] It is well-known that the combined geometric and electronic effects are the key reasons for cooperative and synergistic catalytic performances between two metals present in the catalysts.[7-10] For example, Ni-Mo bimetallics supported on different metal oxides were found to

exhibit enhanced activity particularly in hydrodeoxygenation and dehydrosulfurization reactions.[11-15] Although many reports are available in the open domain, the Mo-Ni synergism explained is limited to very few supports (mainly Al₂O₃) and still there is significant scope for the improvements in this area when Ni-Mo is supported on different metal oxides and zeolites.

In our earlier studies, it was found that the Ni and promoted-Ni species had shown promising activity towards the production of valeric acid (VA) and γ-valerolactone (GVL) from levulinic acid (LA) derived from biomass.[16,17] In addition, many reports appeared on the catalyst development for the LA hydrogenation to GVL and the GVL conversion to VA and its esters.[18-22] In this view, as GVL production from raw biomass rather than from LA is feasible, further conversion of GVL to valerate esters could be an important transformation as esters of VA (such as ethyl valerate; EV) show better and promising fuel blending properties than GVL.[23,24] Very few investigations were reported on GVL conversion in liquid phase at high pressures over the Ni, Ru and Pt-based catalysts, and studies of GVL conversion in continuous-flow mode are rather scarce.[25-27] Therefore, a detailed understanding of the GVL ring opening mechanism to EV over the non-noble metals such as Ni-based catalysts is an area that needs to be studied under continuous-flow conditions at ambient pressure which is also environmentally friendly and beneficial in terms of efficiency, reduced likelihood of catalyst deactivation and cost.[28,29]
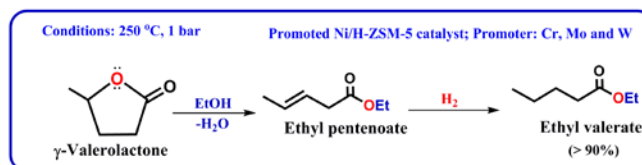
Scheme 1. Catalytic conversion of γ-valerolactone to ethyl valerate.

It is known from former studies that for effective GVL conversion bifunctional catalysts are needed possessing balanced acid and hydrogenation functionalities.[27] Thus, Brønsted acidic H-ZSM-5 was proved to be a suited support material for Ni and other metal supported catalysts because other kinds of supports (SiO₂, Al₂O₃, other zeolites) were less effective in GVL ring opening reaction.[17,20,28]

Therefore, taking advantage of our previous experience on supported Ni catalysts explored in different biomass conversions in vapour phase,[28,30,31] herein we report on Mo, W,

[a] Dr. V.K. Velisoju, Dr. U. Bentrup, Prof. A. Brückner
Leibniz-Institut für Katalyse e. V. (LIKAT)
Albert-Einstein-Str. 29a, 18059 Rostock, Germany.
E-mail: ursula.bentrup@catalysis.de
vijay.velisoju@catalysis.de & velisoju.sva@gmail.com

[b] Dr. D. Jampaiah and Prof. S.K. Bhargava
Centre for Advanced Materials and Industrial Chemistry (CAMIC), School of Science, RMIT University, GPO BOX 2476, Melbourne, VIC 3001, Australia.

[c] Dr. G. Naresh and Dr. A. Venugopal
Catalysis and Fine Chemicals Division, CSIR - Indian Institute of Chemical Technology (IICT) Hyderabad-500 007, Telangana, India.
E-mail:akula.iict@gov.in

Supporting information for this article is given via a link at the end of the document.

and Cr promoted Ni/ZSM-5 catalysts used for the ring opening-hydrogenation of GVL to ethyl valerate (EV; fuel blender) at 250 °C under ambient pressure conditions (Scheme 1). The different impact of the promoters on catalytic activity of Ni/ZSM-5 are explained using bulk and surface characterization methods as well as *in situ* FTIR spectroscopy to study GVL adsorption and its reaction with ethanol. Based on the characterization and *in situ* spectroscopic results, a reaction mechanism was proposed and activities were rationalized.

Results and Discussion

Activity measurements

The catalytic activity results in the conversion of γ-valerolactone (GVL) to ethyl valerate (EV) at 250 °C under ambient pressure are reported in Table 1. To enable reliable comparison of all the catalysts, catalytic tests were performed at almost similar conversion levels (~ 10%).

Table 1. Activity results of GVL conversion to EV over promoted Ni/HZ5 catalysts at 250 °C, GHSV = 5.4 mL g_{cat}^{-1} s^{-1}.

Catalyst	X_{GV} %	S_{EV} %	S_{VA} %	S_{others} [a] %	$Rate_{EV}$ μmol g_{cat}^{-1} s^{-1}
Ni/HZ5	9.1	58.6	26.3	15.1	0.25
Cr-Ni/HZ5	8.6	68.5	19.3	12.2	0.27
Mo-Ni/HZ5	9.6	92.0	3.6	4.4	0.43
W-Ni/HZ5	9.1	80.2	13.2	6.6	0.31
Mo-Ni/HZ5[b]	14.6	75.6	20.5	3.9	0.53
Mo-Ni/HZ5[c]	99.2	91.5	4.2	4.3	0.45
Mo-Ni/HZ5[d]	90.5	85.4	6.6	8.0	0.38
Mo-Ni/HZ5[e]	98.7	91.2	5.1	3.7	0.44

[a] Include 1,4-pentane diol, 4-hydroxyl-ethyl valerate, and ethyl pentenoate. [b] Reaction temperature 300°C. [c] GHSV = 0.54 mL g_{cat}^{-1} s^{-1} at 250 °C. [d] After 50 h reaction time at 250 °C. [e] After catalyst regeneration.

The results showed that all four catalysts are able to produce EV from GVL owing to the presence of acid (Lewis and Brønsted for dehydration and ring opening respectively) and metal sites (for hydrogenation) as demonstrated in the next paragraphs. However, significant changes in the EV selectivity are observed due to the different active site compositions in the promoter-modified Ni on H-ZSM-5 (HZ5) catalysts. The selectivity of EV decreases in the following order: Mo-Ni/HZ5 > W-Ni/HZ5 > Cr-Ni/HZ5 > Ni/HZ5. Apart from EV, valeric acid (VA) is another major product observed in the reaction mixture, as it is a known fact that the presence of Brønsted acid sites will also initiate the ring opening of GVL to form VA.[28] However, the

concentration of VA is found to vary between the three promoter-modified Ni/HZ5 catalysts and is lowest for Mo-Ni/HZ5. To see the influence of reaction temperature, the reaction was also carried out at 300 °C over the Mo-Ni/HZ5 sample, whereby a slight increase in GVL conversion was observed. However, a drop in EV selectivity was seen mostly due to the formation of VA. This result confirms that the GVL ring opening is more rapid and selective towards VA rather EV at high temperature. As anticipated, the increase in catalyst weight (low GHSV at 250 °C) showed no significant change in EV selectivity with >99% GVL conversion.

In comparison to other studies, very few researchers reported GVL conversion to ethyl valerate in batch reactor over supported metal catalysts (Table S1).[20,23,27] Comparable EV yield (>90%) is achieved in the present study at atmospheric pressure relative to the reported yields obtained over the supported Pt, Cu, Co and Ru catalysts at 10-40 bar pressure.

The long-term stability test carried out at 250°C under ambient pressure (Table 1) indicated the robustness of Mo-Ni/HZ5 even after 50 h of continuous operation with a slight decrease in EV rate most likely due to the adsorption of reactant/intermediate molecules.[31] However, regeneration in 5% H_2/He flow for 1 h at 450 °C restored its activity (Table S2) with no significant changes in the catalyst structure as evidenced from XRD analysis of fresh and reused Mo-Ni/HZ5 samples (Figure S1).

Powder XRD studies

The XRD analysis of reduced catalysts show diffraction signals assigned to Ni in metallic form (Figure 1) with characteristic peaks at 2θ = 44.6, 52.1 and 76.4 (ICDD: 00-004-0850).
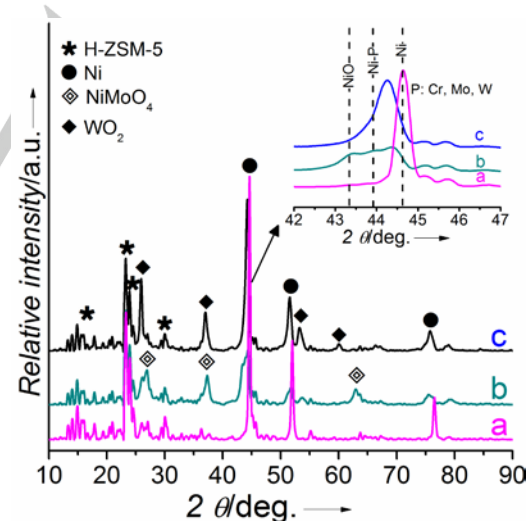

Figure 1. Powder XRD analysis of promoted Ni/HZ5 samples: a) Cr, b) Mo and c) W.

The W promoted Ni/HZ5 (crystallinity = 94.6%) exhibited broad diffraction lines for Ni^0 phases indicating the interaction of W with Ni. This effect seems to be more pronounced in the Mo-Ni/HZ5 sample (crystallinity = 96.3%), where a line broadening of the

Ni(111) plane is observed, and three diffraction signals assigned to the metallic, ionic and promoter interacted Ni phases can be identified (Figure 1, inset). In the absence of promoter, mainly metallic Ni phases were found in the XRD pattern of Ni/HZ5 catalyst (Figure S1).

In the comparative analysis, only the Mo-promoted sample exhibits a $NiMoO_4$ phase (ICDD: 00-033-0948). In the Cr-promoted Ni/HZ5 sample (crystallinity = 93.1%), no diffraction signal can be seen from either isolated chromium oxide or mixed-oxide phases, whilst in the W-promoted sample WO_2 (ICDD: 01-081-7048) can be detected in the reduced samples. A small shift of the diffraction signals of metallic Ni to lower angle with Mo addition suggests that the Mo atom, having larger size than the Ni atom, is incorporated into Ni forming a Mo-Ni mixed metal-oxide phase.[32] Though, a small shift of the Ni planes is also evident in W-promoted sample due to interaction of Ni with W, a mixed metal-oxide phase is not detected in the W-modified Ni/HZ5 catalyst (below the XRD detection limit).

Physico-chemical properties

Some physico-chemical characteristics are summarized in Table 2. The BET-surface area (S_{BET}) analysis of the catalysts showed no significant differences between the catalysts after Ni and promoter impregnation, mostly due to the fixed quantity of Ni and promoters on the support, which is also true with the H_2 uptakes of the catalysts obtained from H_2-TPR analysis. In addition, the NH_3-uptake values obtained from NH_3-TPD analysis revealed a slightly higher amount of surface acidity on W-Ni/HZ5 and Mo-Ni/HZ5 samples. The ratio of Brønsted acid sites (BAS) and Lewis acid sites (LAS) is comparable for the W and Cr promoted catalysts, but is essential lower in the case of Mo-Ni/HZ5.

Table 2. Physico-chemical characteristics of promoter modified Ni catalysts.

Catalyst	S_{BET} $m^2 g^{-1}$	H_2-TPD[a] $\mu mol\ gcat^{-1}$	NH_3-TPD $\mu mol\ g\ cat^{-1}$	S_{Ni}[b] $m^2 g_{metal}^{-1}$	B/L[c]
Cr-Ni/HZ5	283	1364	1.90	22.3	0.22
Mo-Ni/HZ5	286	1455	2.71	14.5	0.12
W-Ni/HZ5	280	1462	2.14	20.1	0.21

[a] H_2 uptake calculated from TPR curves, calibrated with Ag_2O.
[b] Calculated using CO uptakes obtained from CO-pulse chemisorption.
[c] Ratio of Brønsted (B) and Lewis (L) acid sites determined from pyridine FTIR measurements.

The H_2-TPR was used to investigate the reduction behaviour of the catalysts (Figure 2) and the respective H_2-uptakes are given in Table 2. At least two major signals were found in all samples. The main signal in Cr-Ni/HZ5 at 382 °C can be assigned to the reduction of NiO significantly interacting with HZ5. [17, 33] A small hump observed at low temperature ~ 150 °C is due to the oxidic Cr species reduction originating from the Cr^{x+} species in a higher oxidation state (3 >x<6) in the form of isolated chromate species

dispersed on the support.[34] In the case of Mo and W promoted samples, the first signal is assigned to reduction of surfacial NiO interacting with the support and the second one present at high temperature can be assigned to reduction of promoted (Mo or W) NiO and/or bulk NiO species strongly interacting with the support material.[17, 35]
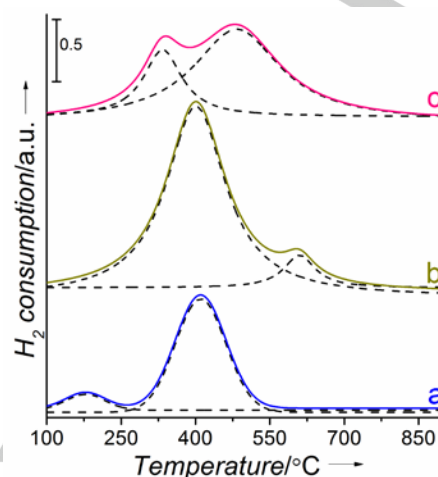

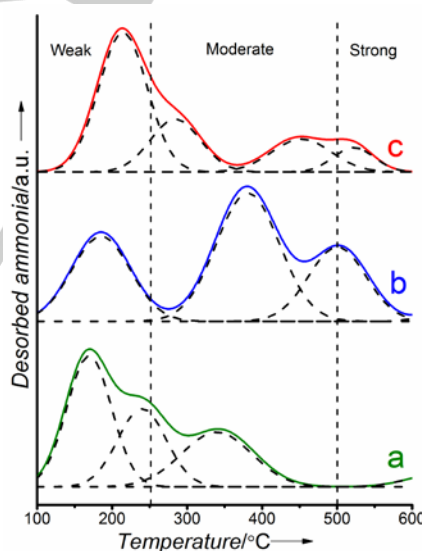Figure 2. H_2-TPR profiles of promoted Ni/HZ5 samples: a) Cr, b) Mo and c) W.

Figure 3. NH_3-TPD profiles of a) Cr, b) Mo and c) W promoted Ni/HZ5 catalysts.

The strength and distribution of acid sites on the surface of the catalysts were studied using NH_3-TPD analysis (Figure 3). The obtained results revealed three regions depending on the adsorption strength of NH_3 at different temperatures *viz.* weak (<250 °C), moderate (250-500 °C) and strong (>500 °C) acid sites. Both Mo and W promoted samples exhibit peaks in all three types of acidic regions while the Cr-promoted sample

shows only weak and moderate acidic sites. Additionally, it is worth noticing that the proportion of moderate-strong acid sites is relatively higher in the Mo-Ni/HZ5 sample compared to the Cr and W modified catalysts.

HR-TEM images of the un-promoted, as well as the Cr-, W- and Mo-promoted Ni/HZ5 catalysts are shown in Figure 4. It was found that the Ni nanoparticles are well dispersed on the surface of HZ5. The presence of Ni species can be concluded from the observed lattice plane distance of 0.201 nm being characteristic of the Ni(111) plane.[36] Interestingly, Cr-modified Ni/HZ5 catalyst did not exhibit lattice planes related to the CrO_x phases, which can be due to its amorphous nature as also concluded from XRD analysis (Figure 1). Furthermore, there are different lattice plane distances other than that of Ni(111) presented in Mo and W promoted Ni/HZ5 catalysts. The lattice plane distance of 0.271 nm can be attributed to the (001) plane of a $NiMoO_4$ phase,[37] whereas for WO_2 (010) lattice plane distance of 0.379 nm was determined.[38] These results are therefore in well accordance with the results obtained from XRD and XPS analysis of the catalysts confirming the presence of a mixed-metal oxide phase only in Mo promoted Ni/HZ5 catalysts.
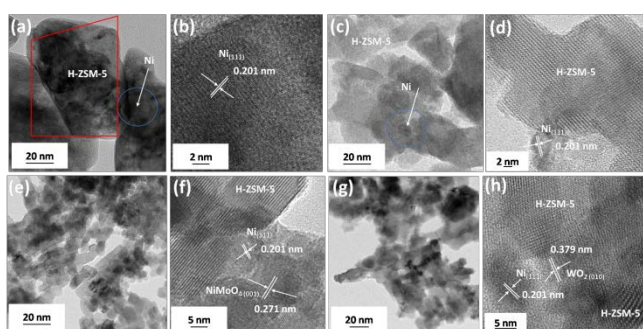

Figure 4. HR-TEM images of (a,b) Ni/HZ5, (c,d) Cr, (e,f) Mo, and (g,h) W modified Ni/HZ5 catalysts..

The surface characteristics of Cr, Mo and W promoted Ni/HZ5 samples were examined using XPS (Figure 5). XPS spectra exhibited two types of Ni species present in Cr and W promoted catalysts. The signals at ~ 852.4 eV and ~ 855.6 eV (with a satellite signal at ~ 861.3 eV) are related to Ni species in metallic and ionic forms, respectively.[39] In contrast, the Mo promoted catalyst exhibits an additional signal at ~ 854.2 eV (satellite at ~858.1 eV) assigned to a Ni species interacting with Mo. These results are in good accordance with the XRD results of the Mo-Ni/HZ5 catalyst, in which three types of Ni species have been observed for the Mo promoted Ni/HZ5 catalyst. It should also be noted that the significant proportion of ionic Ni (NiO form) in all the catalysts is not only caused by incomplete reduction but is also related to surface oxidation of Ni during the sample transfer and exposure to ambient atmosphere before XPS analysis.[40] The surface analysis (XPS) showed no significant well resolved peaks for interacting nickel species in the Cr and W promoted Ni/HZ5 samples. This further supports that alloy formation is more apparent in both the bulk and on the surface of the Mo-

Ni/HZ5 catalyst compared to the other catalysts. Furthermore, a well resolved O 1s (Figure S2) spectrum is also observed in the Mo-Ni/HZ5 catalyst compared to the Cr and W promoted catalysts.
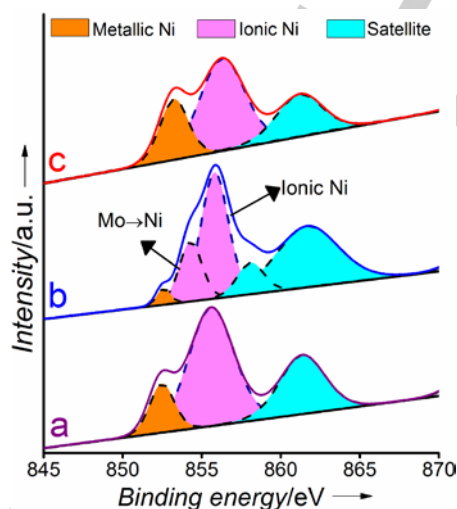

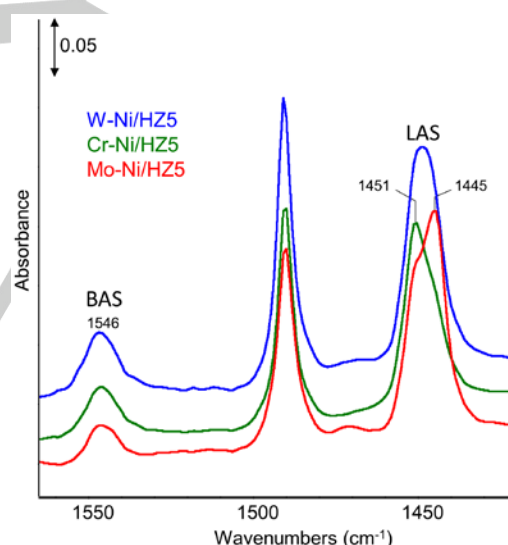**Figure 5.** XPS Ni 2p spectra of promoted Ni/HZ5 samples: a) Cr, b) Mo, c) W.

Figure 6. Pyridine adsorbate spectra of pre-reduced promoted Ni/HZ5 catalysts recorded at 150°C.

In addition to the surface Ni species, the nature of promoter species (Cr, Mo and W) on the catalyst surface has also been investigated by XPS (Figure S3).[41-43] The surface composition obtained from XPS analysis revealed a relatively high ratio of Mo/Si as compared to Cr/Si and W/Si ratios (Table S1). This clearly indicates that Cr (mostly isolated Cr_xO_y phase) and W (isolated W_xO_y species) are present predominately in the bulk and to a lower extent on the surface, whereas Mo (mainly as

mixed metal-oxide phase) is present on both at the surface and in the bulk. Additionally, a well resolved spectrum can be seen for the Mo 3d spectra while broad peaks are observed for both Cr 2p and W 4f, most likely due to the presence of oxidic species in different oxidation states.

Pyridine adsorption with FTIR spectroscopy has been used to characterize the nature of acid sites (Brønsted and/or Lewis). The pyridine adsorbate spectra (Figure 6) show significant proportions of both types, pyridine coordinated to Lewis acid sites (LAS) and protonated pyridine (BAS) on all catalysts indicated by the typical bands at ≈1450 cm^{-1} and ≈1540 cm^{-1}, respectively.[44, 45] A relatively high amount of acid sites has been detected on Mo-Ni/HZ5 which is in accordance with the NH$_3$-TPD results, while the ratio of BAS/LAS is the lowest in Mo-Ni/HZ5 (Table 2). It is also interesting to notice that the LAS band of the Mo-Ni/HZ5 and the Cr-Ni/HZ5 samples exhibit two components at 1445 and 1451 cm^{-1} indicating the presence of LAS with different strength. Thus, the percentage of sites of lower strength (1445 cm^{-1}) is higher on Mo-Ni/HZ5. Only one, but broad LAS band is observed in the W promoted sample indicating the possible presence of two types of LAS, too.

In situ FTIR studies

To study the interaction with GVL under reaction conditions, GVL was directly dosed into the reaction cell which was flushed with 5% H$_2$/He. The adsorbate spectra of the pre-reduced catalysts measured after 15 min contact with GVL at 250 °C are displayed in Figure 7. For comparison, also the spectrum of GVL is shown measured under the same conditions without catalyst in the reaction cell.

The characteristic $\nu_{(C=O)}$ band of GVL is observed at 1786 cm^{-1} shifting to lower wavenumbers due to adsorption.[46] Thus, additional bands around 1765, 1741, and 1694 cm^{-1} appear which indicate weak and strong interactions of GVL with the catalyst surface, respectively.[46, 47] By inspecting the OH region of the FTIR spectra, it can be seen that the OH groups at the surface are involved in this interaction with GVL (Figure S4). Interestingly, an additional broad band around 1558 cm^{-1} is observed on Mo-Ni/HZ5, possibly stemming from an enolate-like adsorbed species. Thus, such band position is also described for metal ketoenol chelate complexes of β-diketones and it is likely that particularly Ni^{2+} Lewis sites as present in Mo-Ni/HZ5 favour the formation of such species.[48, 49] Such types of intermediates were also postulated for the hydroconversion of GVL over Co/SiO$_2$.[46]

After the pre-adsorption of GVL, ethanol was injected into the IR cell to initiate the reaction of GVL ring opening to EV. The reaction progress was followed for 40 min, while the cell was permanently flushed with 5% H$_2$/He. The measured spectra in the carbonyl stretching region are exemplarily shown for the Mo-Ni/HZ5 sample in Figure 8. The respective overall spectra are shown in Figure S5. Immediately, after dosing ethanol, the intensity of the bands of adsorbed GVL decreases and a new band at 1738 cm^{-1} emerges which stems from a carbonyl vibration of a product formed by the reaction of adsorbed GVL with ethanol. It is most likely that this band is related to the carbonyl stretching vibration of ethyl valerate, because for ethyl

propanoate and ethyl butanoate carbonyl bands were found in the same spectral region around 1738 cm^{-1} and 1744 cm^{-1}, respectively.[50]
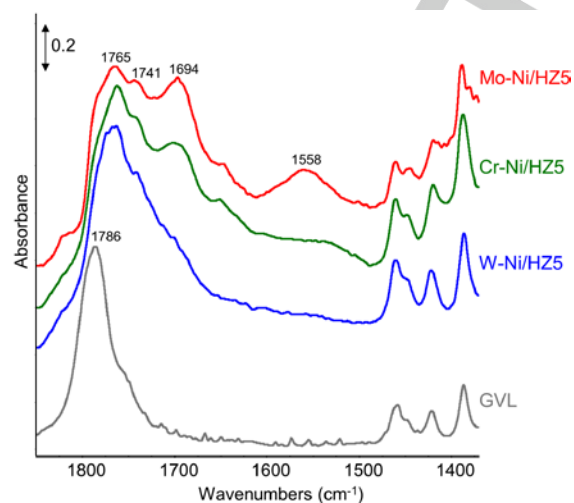

Figure 7. GVL adsorbate spectra of promoter modified Ni/HZ5 catalysts recorded after 15 minutes of contact with GVL at 250°C. For comparison the spectrum of pure GVL is also shown.
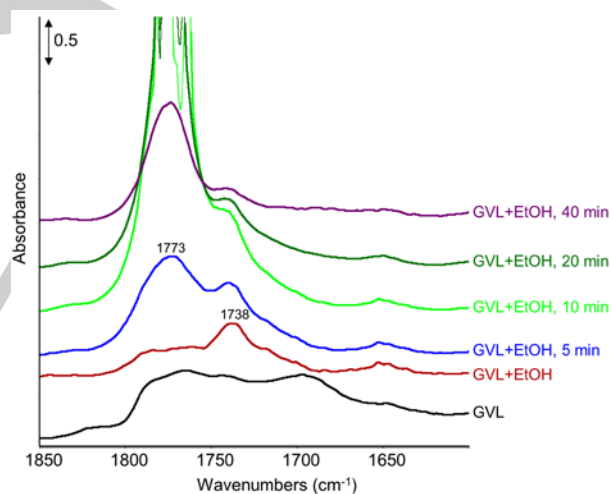

Figure 8. *In situ* FTIR spectra of Mo-Ni/HZ5 measured after GVL adsorption and subsequent ethanol injection at 250°C under flushing with 5% H$_2$/He.

After 5 min an additional band at 1773 cm^{-1} appears, the intensity of which increases dramatically after 10 min. This band stems most probably from valeric acid (VA) because of the comparable high frequency of the carbonyl band. In the spectra measured after 10 and 20 min also rotational bands are observable, which means that VA is mainly in the gas phase. This finding is in accordance with the catalytic testing results, where VA was found as the main side product. Because the FTIR reaction cell was continuously flushed with 5% H$_2$/He, after 40 min only the

bands of adsorbed species can be observed which belongs to mainly VA and EV.

Comparing the spectra of all catalysts measured after GVL pre-adsorption and subsequent dosing of ethanol a similar behaviour was observed (Figure 9, Figure S6). For all catalysts the intensities of the bands of adsorbed GVL decrease and a band at 1738 cm^{-1}, assigned to the carbonyl vibration of ethyl valerate, appears. However, this band is distinctly more intensive on Mo-Ni/HZ5. This suggests a higher activity of this catalyst compared to the other ones, which is in accordance with the catalytic testing results (*cf.* Table 1).
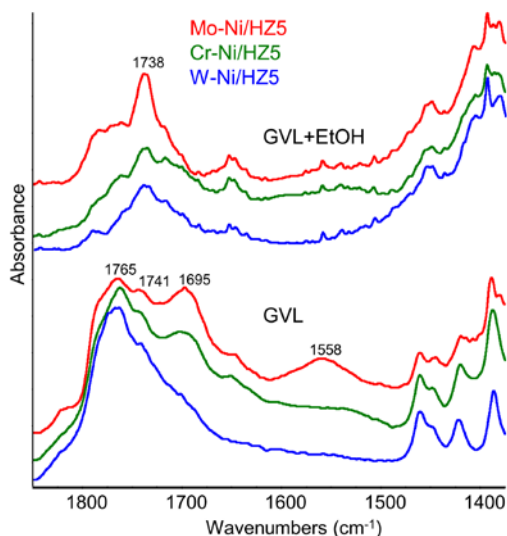

Figure 9. Normalized *in situ* FTIR spectra of the promoted Ni/HZ5 catalysts measured after GVL adsorption (bottom) and subsequent ethanol injection at 250°C (top).

Summarizing the results of *in situ* FTIR spectroscopic studies it can be stated that GVL is strongly adsorbed on all catalysts studied as indicated by the shift of the carbonyl band to lower wavenumbers. Over Mo-Ni/HZ5 additionally enolate-like species were observed the formation of which seems to be favoured by Ni^{2+} Lewis sites most probably existing in the NiMoO$_4$ phase. Hence, the enol form of GVL interacts with Lewis sites via a chelate like coordination while hydroxyl groups are formed on the nickel molybdate phase.

After dosing ethanol, EV is quickly formed, while with reaction progress the formation of VA is observed. Considering that all injected ethanol is consumed in the reaction with adsorbed GVL, the formation of the free acid is preferred as long as adsorbed GVL is present, because the reaction cell was flushed with H$_2$/He during the experiment.

According to the above results and discussions, a plausible reaction mechanism for GVL ring opening can be proposed which is in good agreement with results reported in other studies.[17,46,51] It is worth noticing that the reaction proceeds through two pathways as depicted in Scheme 2, with path I being more predominant over all studied catalysts. This is obviously due to the fact that all catalysts possess both Brønsted as well as Lewis acid sites which favour reaction path I.[46] However, concerning the product distribution from catalytic testing, where also 4-hydroxy-ethyl valerate and 1,4-pentane diol were detected, pathway II cannot be excluded.
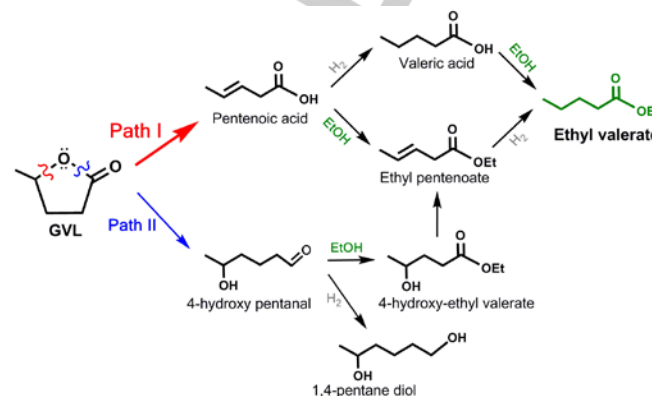
Scheme 2. Proposed reaction pathways for GVL conversion over metal-promoted Ni/HZ5 catalysts.

As also suggested by Novodárszki et al.[46] and Lange et al.[27] besides Brønsted acid sites for ring opening hydrogenation functionalities provided by metallic sites are needed to convert firstly formed pentenoic acid to VA. For preferring this pathway acid and hydrogenation functions have to be well balanced to push pentenoic acid formation. In this regard the metal loading plays an essential role.[27] Thus, low metal loading favours the formation of pentenioc acid, while high metal loading provoke the formation of 2-methyl hydrofuran and other over-hydrogenated products. This, in turns means for the metal promoted Ni/HZ5 catalysts, that at constant metal loading but varying metals the reducibility of the different catalysts plays an important role for creating the metallic hydrogenation functions. Comparing the physico-chemical characteristics of the promoted Ni/HZ5 catalysts (*cf.* Table 2) it is evident that the Mo-Ni/HZ5 has the lowest S$_{Ni}$ and the lowest BAS/LAS ratio which is obviously related to the presence of the NiMoO$_4$ phase. However, this catalyst revealed the best catalytic performance which suggests that an optimal ratio of acid and hydrogenation functions is realized here.

Conclusions

The synergistic interactions between Ni and promoter (Cr, Mo and W) supported on H-ZSM-5 were investigated in γ-valerolactone (GVL) ring opening and its conversion to ethyl valerate (EV) in the vapor phase. Depending on the used promoter significant changes in the EV selectivity are observed which is due to the different active site compositions. While three types of Ni species, metallic, ionic, and promoter interacted Ni exist in the Mo-Ni/HZ5 catalyst besides a mixed metal oxide phase NiMoO$_4$, only two types of Ni species were observed for

the Cr and W modified catalysts while no mixed oxide phases were formed. This suggests that the high activity obtained over the Mo-promoted Ni/HZ5 catalyst is due to the specific Ni-Mo synergy leading to comparable low Ni^0 surface area along with a lower BAS/LAS ratio compared to the other promoted catalysts.

The results of *in situ* FTIR studies revealed a different strength of GVL adsorption on the promoted catalysts being strongest on Mo-Ni/HZ5 surface, which might be favored by the presence of Ni^{2+} Lewis sites existing in the $NiMoO_4$ phase. Pre-adsorbed GVL reacts quickly with ethanol by formation of EV the concentration of which is the highest on Mo-Ni/HZ5, in accordance with the catalytic testing results. When all injected ethanol is consumed the formation of the VA is preferred as long as adsorbed GVL is present.This suggests a ring opening reaction rather via pentenoic acid than via 4-hydroxy pentanal as intermediate. Taking into account that Brønsted acid sites are needed for ring opening and metallic sites for providing hydrogenation functionalities to convert firstly formed pentenoic acid to VA and EV, an optimal ratio of acid and hydrogenation functions seems to be important as also suggested by other authors. This might be realized in Mo-Ni/HZ5, which has the lowest S_{Ni} and BAS/LAS ratio most probably caused by the presence of the $NiMoO_4$ phase.

Experimental Section

Following chemicals (A. R. grade; 99.9%) were purchased from Sigma-Aldrich: $Ni(NO_3)_2 \cdot 6H_2O$, $Cr(NO_3)_2 \cdot 9H_2O$, $(NH_4)_6Mo_7O_{24} \cdot 4H_2O$ and $(NH_4)_{10}W_{12}O_{41} \cdot xH_2O$. γ-Valerolactone (GVL; 99%), valeric acid (VA; 99%), ethyl valerate (EV; 99%), ethanol (>99%) and pyridine (99.8%) was used as received. H-ZSM-5 (HZ5; Si/Al = 40; S_{BET} = 413 m^2 g^{-1}) obtained from M/s. Alfa Aesar was used as support.

The Cr, Mo and W promoted Ni/HZ5 catalysts containing 10 wt% Ni and 2 wt% of the respective promoter metal were synthesized by a co-impregnation method. In this method, impregnation of metal on the support was performed with the aqueous salt containing the corresponding amount of $Ni(NO_3)_3 \cdot 6H_2O$ (10 wt%) and/or the promoter (Cr, Mo and W) precursors (2 wt%) mixed with the desired amounts of HZ5 support with stirring at 100 °C followed by drying the samples for 12 h at 120 °C. Then the calcination step was performed at 450 °C in static air for 5 h. The elemental composition of the catalysts was determined by the ICP-OES analysis and is given in Table S3 and the contents of metals were given in weight percentages.

Activity tests were performed in a fixed-bed quartz reactor in continuous-flow mode at atmospheric pressure. Prior to testing, the samples (0.1 – 1 g, sieved particles of catalyst) were *in situ* reduced at 450 °C for 3 h in 5% (v/v) H_2/Ar. The reactant mixture consisting of GVL (10 wt%) in ethanol was then fed into the reactor and vaporized in the pre-heating zone at 250 °C. The reaction zone containing the catalyst was sand-wiched between quartz wool plunges. The reaction was carried out at 250 °C with 2 mL h^{-1} flow rate of the reactant along with H_2 flow. The product mixtures were collected using an ice-cold trap and analysed using a gas chromatograph (GC) equipped with an FID and capillary wax column for quantitative information. The products were identified using a GC equipped with mass spectrometer (MS) detector. The gas phase analysis was performed by connecting the outlet of the reactor directly to GC-TCD. The detailed experimental conditions are also provided in the supporting information.

X-ray diffractometer (Bruker D4 Endeavor wide angle) was used to obtain the powder X-ray diffraction (XRD) patterns of the catalysts using Ni filtered Cu Kα radiation (2 θ: 5-80°scan rate: 5° min^{-1}).

The N_2 physisorption experiments were carried out for all the catalysts to determine the surface area using N_2 adsorption at -196 °C, in Micromeritics surface area analyser. The samples were degassed at 250 °C for 12 h in N_2 flow prior to the physisorption experiment. Specific surface areas (m^2 g^{-1}) were calculated applying BET (Brunauer-Emmett-Teller) method.

The temperature programmed reduction (TPR) studies were carried out in a quartz micro-reactor connected to a gas chromatograph (GC). The loaded catalyst was subjected to degassing at 300 °C in He gas flow to remove the moisture. The furnace was cooled to room temperature after degassing and the He gas was switched to 4.97% H_2 in Ar and the temperature was programmed to reach the maximum. The Ag_2O-TPR calibration curve was used to obtain the H_2 consumption of the catalysts.

The acid site distribution of catalysts was studied on a Micromeritics device by temperature programmed desorption (TPD) of ammonia. The catalyst sample was in situ reduced at 450 °C in H_2/Ar for 1 h. The furnace temperature was brought down to 100 °C. The catalyst surface was then saturated with NH_3 followed by flushing the sample in He flow to eliminate the physically adsorbed ammonia. The furnace temperature was again raised to maximum to carry out the ammonia desorption and distribution of acid site was obtained from the total amount of desorbed ammonia.

The CO-pulse titration procedure was employed to measure the active metal surface area of the catalysts at 40 °C in a gas sorption analyser. The samples were *in situ* reduced for 2 h at 450 °C and then flushing the catalyst in He flow for 1 h. The CO pulses were then injected until saturation. The CO uptake was obtained using a GC with a thermal conductivity detector and Carboxen-1000 column. The active metal surface area was calculated according: Metal area = Metal cross sectional area x No. of metal atoms on surface, by assuming the stoichiometry of CO: metal = 1:1.[52]

The surface oxidation states of elements and their surface composition was studied by the X-ray photoelectron spectroscopy (XPS) analysis on the X-ray photoelectron spectrometer (Thermo K Alpha, Al Kα X-ray excitation source; E_{photon} = 1486.7 eV). Carbon signal at 284.6 eV (C 1S) was used as a reference to correct the binding energies. Shirley method was employed for the background subtraction and the spectrum fitting (for each peak) was done with a linearly combined Gaussian functions using Avantage-XPS software.

HR-TEM images of the reduced catalysts were obtained with JEOL 2100F TEM with Gatan OneView 4k CCD Camera. The samples were prepared by grinding them in a mortar followed by dispersion in iso-propanol via sonication. Then a drop of the suspension aliquot was placed on a carbon-coated copper grid and allowed it to dry by evaporation at an ambient temperature.

In situ FTIR studies were performed in transmission mode on a Bruker Tensor27 spectrometer for pyridine adsorption and on a Thermo Scientific Nicolet 6700 spectrometer for GVL adsorption. Both spectrometers were equipped with respective home-made heatable and evacuable reaction cells with CaF_2 windows connected to a gas dosing system. The pre-reduced sample powders were pressed into self-supporting wafers with a diameter of 20 mm and a weight of 50 mg, and were pre-reduced again in 5% H_2/He at 400 °C for 1 h. After cooling to

the desired temperature for probe adsorption, a sample spectrum was recorded. Then, the samples were exposed to subsequent doses of probe molecules (at 25 °C for pyridine and 250 °C for GVL), and spectra were recorded with a resolution of 4 cm^{-1} and 64 scans. Pyridine was dosed via a saturator, while GVL and ethanol were directly injected into the reaction cell which was permanently flushed with 5% H$_2$/He. After pyridine adsorption, the reaction cell was evacuated for removing physisorbed pyridine. Then, desorption of pyridine was followed by heating the sample in vacuum and recording spectra at selected temperatures. Generally, difference IR spectra were analysed, obtained by subtraction of the spectrum of the pre-reduced sample at adsorption temperature from the respective adsorbate spectra.

Acknowledgements

Keywords: γ-Valerolactone• Ethyl Valerate• heterogeneous catalysis• promoted Ni/H-ZSM-5• *in situ* FTIR

[1]   A. E. Aksoylu, Z. Mosorlo, Z. I. Onsan, *Appl. Catal., A.* **1998**, *168*, 385-397.

[2]   R. Nava, B. Pawelec, P. Castaño, M. C. Álvarez-Galván, C. V. Loricera, J. L. G. Fierro, *Appl. Catal., B.* **2009**, *92*, 154-167.

[3]   X. Liu, A. Wang, L. Li, T. Zhang, C. Y. Mou, J. F. Lee, *J. Catal.* **2011**, *278*, 288-296.

[4]   J. Lee, Y. T. Kim, G. W. Huber, *Green Chem.* **2014**, *16*, 708-718.

[5]   Z. Mohamed, V. D. B. C. Dasireddy, S. Singh, H. B. Friedrich, *Appl. Catal., B.* **2016**, *180*, 687-697.

[6]   D. M. Alonso, S. G. Wettstein, J. A. Dumesic, *Chem. Soc. Rev.* **2012**, *41*, 8075-8098.

[7]   I. Sharafutdinov, C. F. Elkjær, H. W. P. Carvalho, D. Gardini, G. L. Chiarello, C. D. Damsgaard, J. B. Wagner, J. D. Grunwaldt, S. Dahl, I. Chorkendorff, *J. Catal.* **2014**, *320*, 77-88.

[8]   J. Ashok, Y. Kathiraser, M. L. Ang, S. Kawi, *Catal. Sci. Technol.* **2015**, *5*, 4398-4409.

[9]   M. M. Lia, S. C. E. Tsang, *Catal. Sci. Technol.* **2018**, *8*, 3450-3464.

[10]   F. Besenbacher, I. Chorkendorff, B. S. Clausen, B. Hammer, A. M. Molenbroek, J. K. Norskov, I. Stensgaard, *Science* **1998**, *279*, 1913-1915.

[11]   T. Borowiecki, W. Gac, A. Denis, *Appl. Catal., A.* **2004**, *270*, 27-36.

[12]   I. Hita, A. Gutiérrez, M. Olazar, J. Bilbao, J. M. Arandes, P. Castaño, *Fuel* **2015**, *145*, 158-169.

[13]   P. Kumar, S. K. Maity, D. Shee, *ACS Omega* **2019**, *4*, 2833-2843.

[14]   S. Mukundan, M. A. Wahab, L. Atand, M. Konarova, J. N. Beltramini, *RSC Adv.* **2019**, *9*, 17194-17202.

[15]   A. Wang, Y. Wang, T. Kabe, Y. Chen, A. Ishihara, W. Qian, P. Yao, *J. Catal.* **2002**, *210*, 319-327.

[16]   V. K. Velisoju, G. Naresh, S. Deepa, P. G. Bhavani, M. Nagaraju, M. Sudhakar, K. V. R. Chary, J. Tardio, S. K. Bhargava, A. Venugopal, *Appl. Catal., A.* **2017**, *531*, 169-176.

[17]   V. K. Velisoju, G. Naresh, J. Tardio, S. K. Bhargava, V. Krishna, C. Anjaneyulu, M. Sudhakar, A. Venugopal, *Appl. Catal., A.* **2018**, *550*, 142-150.

[18]   S. G. Wettstein, J. Q. Bond, D. M. Alonso, H. N. Pham, A. K. Datye, J. A. Dumesic, *Appl. Catal., B.* **2012**, *117-118*, 321-329.

[19]   V. K. Velisoju, P. G. Bhavani, G. Naresh, B. Venu, K. Manasa, K. V. R. Chary, A. Venugopal, *J. Phys. Chem. C* **2018**, *122 (34)*, 19670-19677.

[20]   W. Luo, P. C. A. Bruijnincx, B. M. Weckhuysen, *J. Catal.* **2014**, *320*, 33-41.

[21]   S. Cao, J. R. Monnier, C. T. Williams, W. Diao, J. R. Regalbuto, *J. Catal.* **2015**, *326*, 69-81.

[22]   P. G. Bhavani, V. K. Velisoju, K. Manasa, G. Naresh, K. V. R. Chary, A. Venugopal, *Catal. Today* **2019**, *325*, 68-72.

[23]   P. Sun, G. Gao, Z. Zhao, C. Xia, F. Li, *ACS Catal.* **2014**, *4*, 4136-4142.

[24]   C. E. Chan-Thaw, M. Marelli, R. Psaro, N. Ravasio, F. Zaccheria, *RSC Adv.* **2013**, *3*, 1302-1306.

[25]   I. Obregón, I. Gandarias, A. Ocio, I. García-García, N. Alvarez de Eulate, P. L. Arias, *Appl. Catal., B.* **2017**, *210*, 328-341.

[26]   R. M. Bababrik, B. Wang, D. E. Resasco, *Ind. Eng. Chem. Res.* **2017**, *56*, 3217-3222.

[27]   J. P. Lange, R. Price, P. M. Ayoub, J. Louis, L. Petrus, L. Clarke, H. Gosselink, *Angew. Chem. Int. Ed.* **2010**, *49*, 4479-4483.

[28]   V. K. Velisoju, G. Naresh, S.K. Bhargava, J. Tardio, V. Karnakar, A. H. Padmasri, A. Venugopal, *RSC Adv.* **2016**, *6*, 9872-9879.

[29]   C. Moreno-Marrodan, P. Barbaro, *Green Chem.* **2014**, *16*, 3434-3438.

[30]   V. K. Velisoju, G. Naresh, M. Sudhakar, J. Tardio, S. K. Bhargava, A. Venugopal, *Appl. Catal., A.* **2015**, *505*, 217-223.

[31]   M. Sudhakar, V. K. Velisoju, G. Naresh, M. L. Kantam, S. K. Bhargava, A. Venugopal, *Appl. Catal., B.* **2016**, *180*, 113-120.

[32]   H. Youn, J. G. Seo, P. Kim, I. K. Song, *J. Mol. Catal. A: Chem.* **2007**, *261*, 276-281.

[33]   W. Lin, H. Cheng, L. He, Y. Yu, F. Zhao, *J. Catal.* **2013**, *303*, 110-116.

[34]   V. Krishna, G. Naresh, V. K. Velisoju, M. Suresh, A. H. Padmasri, A. Venugopal, *Catal. Sci. Technol.* **2017**, *7*, 3399-3407.

[35]   J. L. Brito, J. Laine, *J. Catal.* **1993**, *139*, 540-550.

[36]   Z. Jiang, J. Xie, D. Jiang, Z. Yan, J. Jing, D. Liu, *Appl. Surf. Sci.* **2014**, *292*, 301-310.

[37]   B. Chang, J. Yang, Y. Shao, L. Zhang, W. Fan, B. Huang, Y. Wu, X. Hao, *ChemSusChem* **2018**, *11*, 3198-3207.

[38]   Z. Xi, D. P. Erdosy, A. Mendoza-Garcia, P. N. Duchesne, J. Li, M. Muzzio, Q. Li, P. Zhang, S. Sun, *Nano Lett.* **2017**, *17(4)*, 2727-2731.

[39]   M. M. Telkar, J. M. Nadgeri, C. V. Rode, R. Chaudhari, *Appl.Catal., A.* **2005**, *295*, 23-30.

[40]   J. Wang, G. L. Fan, H. Wang, F. Li, *Ind. Eng. Chem. Res.* **2011**, *50*, 13717-13726.

[41]   D. Li, A. Nishijima, D. E. Morrisz, *J. Catal.* **1999**, *182*, 339-348.

[42]   Y. Fan, H. Xiao, G. Shi, H. Liu, X. Bao, *Energy Environ. Sci.* **2011**, *4*, 572-582.

[43]   D. Jampaiah, A. Chalkidis, Y. M. Sabri, E. L. H. Mayes, B. M. Reddy, S. K. Bhargava, *Catal. Today* **2019**, *324*, 174-182.

[44]   H. Knözinger, P. Ratnasamy, *Catal. Rev.* **1978**, *17*, 31-70.

[45]   J. A. Lercher, C. Gründling, G. Eder-Mirth, *Catal. Today* **1996**, *27*, 353-376.

[46]   G. Novodárszki, H. E. Solt, G. Lendvay, R. M. Mihályi, A. Vikár, F. Lónyi, J. Hancsók, J. Valyon, *Catal. Today* **2019**, *336*, 50-62.

[47]   N. Scotti, M. Dangate, A. Gervasini, C. Evangelisti, N. Ravasio, F. Zaccheria, *ACS Catal.* **2014**, *4*, 2818-2826.

[48]   R. P. Dryden, A. Winston, *J. Phys. Chem.* **1958**, *62*, 635-637.

[49]   T. G. Dunne, F. A. Cotton, *Inorg. Chem.* **1963**, *2*, 263-266.

[50]   NIST Chemistry Web Book, SRD69.

[51]   W. Li, Y. Li, G. Fan, L. Yang, F. Li, *ACS Sustainable Chem. Eng.* **2017**, *5*, 2282-2291.

[52]   A. Tanksale, J. N. Beltramini, J. A. Dumesic, G. Q. Lu, *J. Catal.* **2008**, *258*, 366-377.

FULL PAPER

An optimized ratio of acid and hydrogenation functions on the Mo-promoted Ni/H-ZSM-5 catalyst is key in γ-valerolactone ring opening to form ethyl valerate
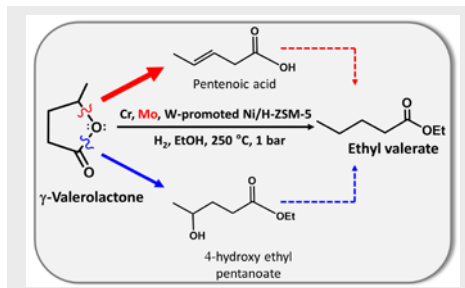
Vijay Kumar Velisoju,* Deshetti Jampaiah, Naresh Gutta, Ursula Bentrup,* Angelika Brückner, Suresh K. Bhargava, and Venugopal Akula*

Page No. – Page No.

Conversion of γ-Valerolactone to ethyl valerate over metal promoted Ni/ZSM-5 catalysts: Influence of Ni0/Ni2+ heterojunctions on activity and product selectivity